

Review

# Rare Earth Ion Doped Luminescent Materials: A Review of Up/Down Conversion Luminescent Mechanism, Synthesis, and Anti-Counterfeiting Application

Ziyu Chen <sup>1,2,\*</sup>, Hang Zhu <sup>1,2</sup>, Jiajie Qian <sup>1,2</sup>, Zhenxiong Li <sup>1,2</sup>, Xiameng Hu <sup>1,2</sup>, Yuao Guo <sup>1,2</sup>, Yuting Fu <sup>1,2</sup>, Huazhong Zhu <sup>1,2</sup>, Wei Nai <sup>1,2</sup>, Zan Yang <sup>3</sup>, Dan Li <sup>3</sup> and Liling Zhou <sup>1,2</sup>

<sup>1</sup> School of Electronic Information, Huzhou College, Huzhou 313000, China

<sup>2</sup> Huzhou Key Laboratory for Urban Multidimensional Perception and Intelligent Computing, Huzhou College, Huzhou 313000, China

<sup>3</sup> Department of Public Education, Huzhou College, Huzhou 313000, China

\* Correspondence: chenzy@zjhzu.edu.cn

† These authors contributed equally to this work.

**Abstract:** With the rapid development of modern technology and information systems, optical anti-counterfeiting and encryption have recently attracted considerable attention. The demand for optical materials is also constantly increasing, with new requirements proposed for performance and application fields. Currently, rare earth ion doped materials possess a unique electronic layer structure, underfilled 4f5d electronic configuration, rich electronic energy level, and long-life excited state, which can produce a variety of radiation absorption and emission. The distinctive properties of rare earth are beneficial for using in diverse optical output anti-counterfeiting. Design is essential for rare earth ion doped materials with multiple responsiveness and multi-channel optical information anti-counterfeiting in the field of information security. Therefore, this mini review summarizes the luminescent mechanisms, preparation methods, performance characteristics and anti-counterfeiting application of rare earth doped materials. In addition, we discuss some critical challenges in this field, and potential solutions that have been or are being developed to overcome these challenges.

**Keywords:** rare earth; luminescence; anti-counterfeiting; structure



**Citation:** Chen, Z.; Zhu, H.; Qian, J.; Li, Z.; Hu, X.; Guo, Y.; Fu, Y.; Zhu, H.; Nai, W.; Yang, Z.; et al. Rare Earth Ion Doped Luminescent Materials: A Review of Up/Down Conversion Luminescent Mechanism, Synthesis, and Anti-Counterfeiting Application. *Photonics* **2023**, *10*, 1014. <https://doi.org/10.3390/photonics10091014>

Received: 27 June 2023

Revised: 24 August 2023

Accepted: 29 August 2023

Published: 5 September 2023



**Copyright:** © 2023 by the authors. Licensee MDPI, Basel, Switzerland. This article is an open access article distributed under the terms and conditions of the Creative Commons Attribution (CC BY) license (<https://creativecommons.org/licenses/by/4.0/>).

## 1. Introduction

Rare earth materials are lanthanide elements with atomic number of 57~71 in the periodic table, as well as yttrium (Y) and scandium (Sc), which possess  $[\text{Xe}]4f^{0-14}5d^{0-1}6s^2$  and  $[\text{Xe}]4f^{0-14}6s^2$  electron configurations. The special electronic configurations endow rare earth materials with luminescence, paramagnetism, and other characteristics [1–3]. The luminescent emission of rare earth ions arises mainly from the f-f transition of 4f electrons and the 4f-5d transition of 4f electrons with 5d electrons. Because the number of 4f electrons varies among different rare earth ions, their electronic transitions and energy level transitions exhibit different forms and are exerted in various luminescence [4,5].

The 4f electrons are less affected by the external crystal field and surrounding environment due to the shielding effect of the outermost electrons on the inner 4f electrons. Therefore, luminescent emission of most trivalent rare earth ions (excluding  $\text{Ce}^{3+}$ ) mainly derives from f-f transitions. The f-f transition possesses linear emission and the spectral band range is wide, which can be extended from the ultraviolet visible region to the near-infrared region [6,7]. Meanwhile, each rare earth ion has a corresponding characteristic emission and insensitive concentration quenching.

In addition, there are some rare earth ions dominated by 4f-5d transitions, which mainly exhibit large absorption intensity, sensitive temperature response, and displaceable emission spectrum. Rare earth ions can also undergo charge transfer state (CTS) transitions

besides f-f and 4f-5d transitions. CTS occurs easily in complexes, and the luminescent emission is generated by the charge transition of ligands to metal ions [8].

Due to their unique electronic layer structure, underfilled external shielding 4f/5d electronic configuration, rich electronic energy level, and long-life excited state, rare earth ions can produce a variety of radiation absorption and emission, constitute a wide range of light and laser materials [9–14]. The luminescence of rare earth almost covers the whole solid luminescent range, achieving incomparable spectral properties. According to current research results in terms of optical applications of rare earth materials, luminescent output and anti-counterfeiting application are at the forefront [15–19].

With the rapid development of social economy and technology, the emergence of counterfeit and inferior goods seriously disrupts the order of the market, and has seriously damaged the interests of consumers. According to incomplete statistics, direct economic losses amount to hundreds of billions of dollars caused by counterfeit products. Counterfeit products circulating in the market, such as drugs, devices, food, etc., have resulted in countless deaths. Therefore, in order to effectively block the spread of counterfeit products, there is an urgent need to develop advanced anti-counterfeiting materials and technologies [20–26].

Current common anti-counterfeiting technologies include paper anti-counterfeiting technology, ink anti-counterfeiting technology, physical anti-counterfeiting technology, biological anti-counterfeiting technology, radio frequency identification (RFID) anti-counterfeiting technology, and so on [27–33]. All anti-counterfeiting technology needs to ensure that it cannot be replicated or imitated. Meanwhile, anti-counterfeiting identification should be easy to inspect and not able to be cracked by third parties within a certain period of time. Among numerous anti-counterfeiting technologies and methods, anti-counterfeiting based on luminescent feature can better meet usage requirements and exhibit more complex performance.

Rare earth ion doped materials with luminescent signal output have received widespread attention from researchers due to their unique and diverse response properties. When a substance is excited (ray, high-energy particle, electron beam, external electric field, etc.) it will be in an excited state, and the energy of the excited state will be released in the form of light or heat [34–36]. Rare earth ion doped materials can absorb energy in a certain way and convert it into light radiation. The performance characteristics of rare earth ion doped materials are well suited for developing application channels for anti-counterfeiting to reduce counterfeit and inferior products, and increase the security of genuine brand products.

## 2. Main Species of Rare Earth Luminescent Materials and Luminescent Mechanism

Rare earth luminescent materials can be classified according to applied range, excitation methods, and emission mode. In terms of applied range, rare earth luminescent materials can be divided into lighting materials, display materials, and detection materials. In terms of different excitation methods, rare earth luminescent materials can be divided into photoluminescent materials, X-ray luminescent materials, electroluminescent materials, and high energy photon excitation luminescent materials. In terms of emission mode, rare earth luminescent materials can be divided into downconversion luminescent materials and upconversion luminescent materials (Figure 1). Luminescence mechanisms will next be introduced, mainly based on the different types of rare earth luminescent materials.

### 2.1. Upconversion Luminescence

Most luminescent materials usually follow the famous Stokes Law, which states that the energy used to excite a photon is greater than the energy used to emit it. However, some luminescent materials also exhibit Anti-Stokes luminescence, where the excitation wavelength is greater than the emission wavelength. Anti-Stokes luminescence is a special optical process that can convert two or more low-energy photons into one high-energy photon and emit it [37–43]. The unique performance is due to the existence of some long-

lived excited state intermediate levels of light-emitting ions, so that light absorption does not start from ground state, but transitions from the intermediate level to a higher excited state level. There are three common upconversion luminescence mechanisms: excited state absorption (ESA), energy transfer upconversion (ETU), and photon avalanche (PA).

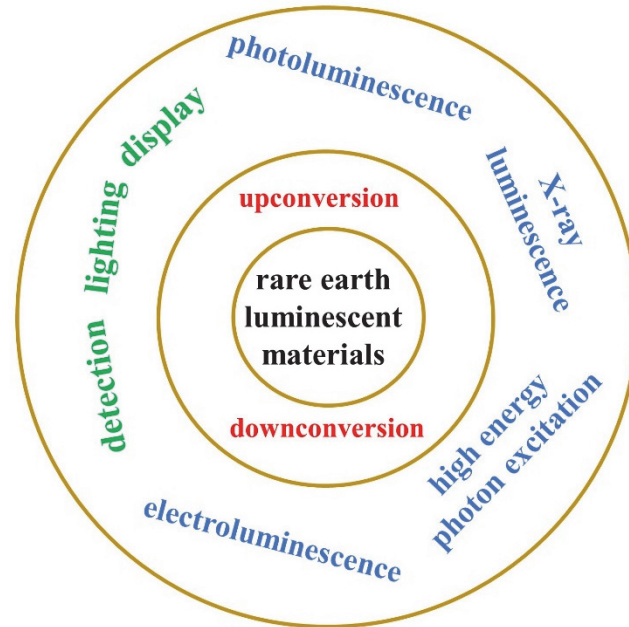


Figure 1. Main species of rare earth luminescent materials.

Figure 2a shows a simple upconversion luminescence mechanism for ESA by a three-level system. The emitted central ion is initially in the ground state (1), and the absorption of the first photon excites it to an intermediate excited state energy level (2). If the ion absorbs a second photon before relaxing back to the ground state, it will be excited to a higher energy level (3). The ion radiation then transitions back to the ground state (1), resulting in the emission of a single photon with higher energy. To achieve ESA, the lifetime must be long enough at energy level (2) and the photon flux must be high enough to absorb the second photon before energy level (2) relaxes back to the ground state.

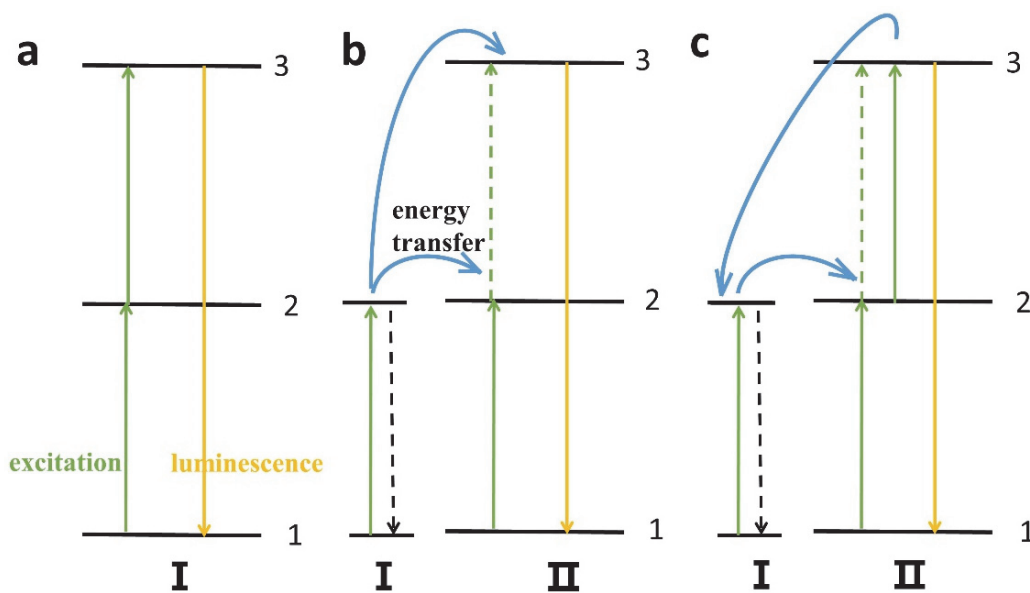


Figure 2. (a) Excited state absorption (ESA), (b) energy transfer upconversion (ETU), and (c) photon avalanche (PA).

In the ETU process, the sensitizer and activator are combined to produce upconversion luminescence. The simplest ETU process is shown in Figure 2b. The sensitizer first absorbs a photon and is excited to the excited state. The energy is transferred (ET) to the activator and promotes ion transitions to the intermediate excited state level (2). The sensitizer transitions back to the ground state without radiation. The second sensitizer absorbs the photon, and the ET excites it to a higher excited state energy level (3) and releases a higher energy photon from that excited state. ET can also occur in conjunction with other processes. For an ETU to be effective, the sensitizer and activator must be close in space for the ET to occur, and the activator energy of the intermediate excited state must be lower than the excited state of the sensitizer, to provide the energy driving force.

The PA upconversion process is mainly based on the cross-relaxation energy transfer (CR-ET) between ions, as shown in Figure 2c. Initially, all ions are in the ground state level (1). Under laser source radiation, the transition process occurs from level (2) to (3) via ESA. Furthermore, through the CR-ET process, the ions can return to level (2), while promoting the entry of adjacent ions into level (2). Ions undergo multiple ESA and CR-ET interactions. Eventually, this progress will lead to an exponential increase in level (2) akin to an avalanche.

NaYF<sub>4</sub> doped with Er<sup>3+</sup> and Yb<sup>3+</sup> is one of the classic upconversion luminescent materials. Typically, 20% of Y<sup>3+</sup> ions are replaced by Yb<sup>3+</sup> and 2% by Er<sup>3+</sup>. The upconversion of NaYF<sub>4</sub>:20%Yb<sup>3+</sup>, 2%Er<sup>3+</sup> is carried out by the ET mechanism, with Yb<sup>3+</sup> as the sensitizer and Er<sup>3+</sup> as the activator, as shown in Figure 3. Under the excitation of a 980 nm laser, the electrons in Yb<sup>3+</sup> transition from <sup>2</sup>F<sub>7/2</sub> to <sup>2</sup>F<sub>5/2</sub>, and the Er<sup>3+</sup> transitions to the <sup>4</sup>I<sub>11/2</sub> energy level through the ET process. Er<sup>3+</sup> undergoes non-radiative relaxation to the <sup>4</sup>I<sub>13/2</sub> level, or a second ET excites it to the <sup>4</sup>F<sub>9/2</sub> level. In addition, a second ET process excites Er<sup>3+</sup> from <sup>4</sup>I<sub>11/2</sub> to <sup>4</sup>F<sub>7/2</sub> and then produces a non-radiative transition to <sup>2</sup>H<sub>11/2</sub> and <sup>4</sup>S<sub>3/2</sub>. Er<sup>3+</sup> radiates back to the <sup>4</sup>I<sub>15/2</sub> from three levels and releases high-energy photons.

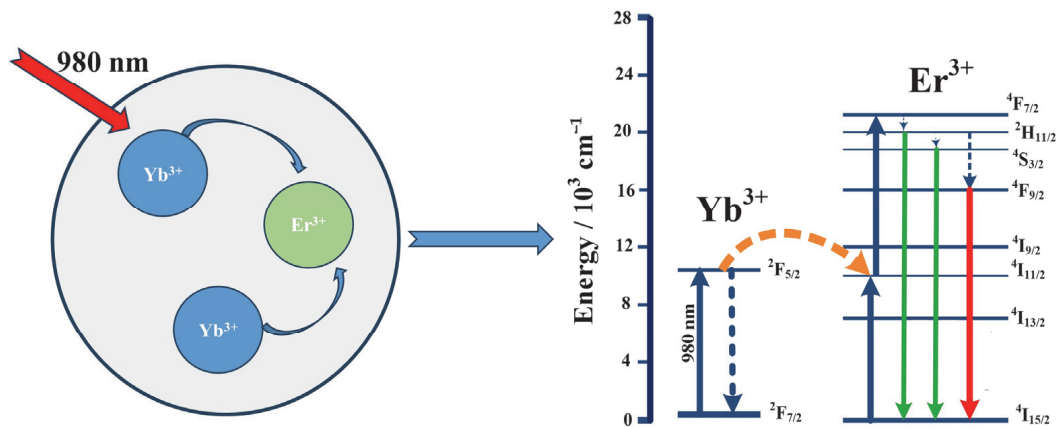


Figure 3. Energy transfer upconversion mechanism in NaYF<sub>4</sub>:Yb<sup>3+</sup>, Er<sup>3+</sup>.

### 2.2. Downconversion Luminescence

Downconversion luminescence follows Stokes Law, which refers to the process of absorbing high-energy photons and converting them into low-energy photons for emission. Downconversion can be divided into downshift and quantum clipping. Downshift means that a high-energy photon can only be absorbed and converted into a low-energy photon. Quantum clipping means that high-energy photon energy is absorbed and converted into multiple low-energy photons [44–48].

The downconversion luminescence mechanism is shown in Figure 4. In Figure 4a, the electron transitions from the ground state to the excited state after absorbing photon energy, and continues to transition and emit light of different wavelengths at different energy levels. In Figure 4b, cross relaxation of electrons occurs between the two ions, accompanied by an energy transfer. After the electrons return to the ground state, fluorescence is released, while the remaining energy is transferred to other ions. The process in Figure 4c is similar to

that in Figure 4b, based on cross relaxation, emitting multiple photons and simultaneously releasing luminescence. In Figure 4d, electrons transition from the ground state to the excited state after absorbing energy, then transition down to the lower excited state and emit low-energy photons. The energy is transferred with other ions to emit visible light when the electrons return to the ground state.

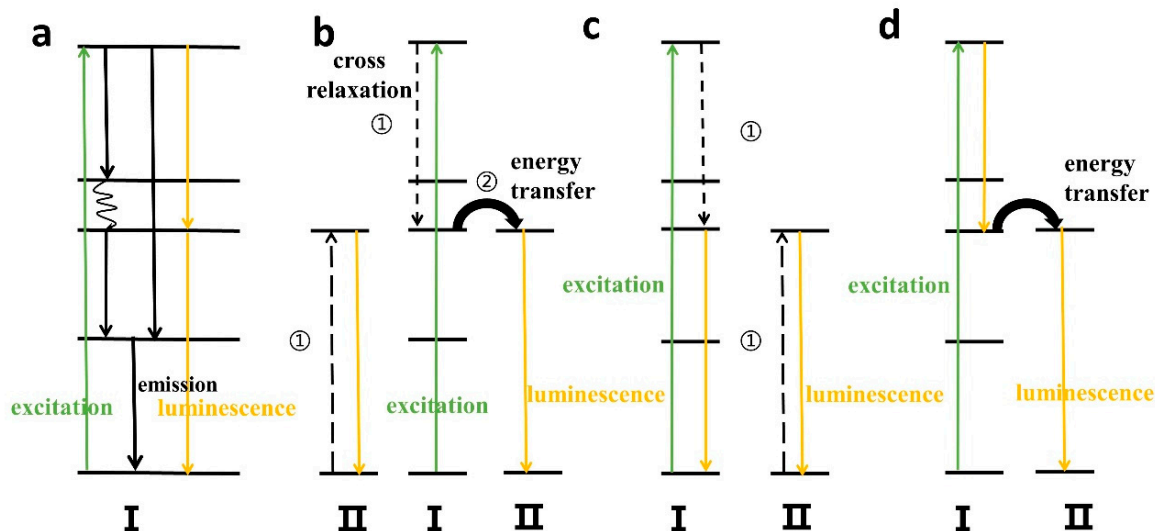


**Figure 4.** Downconversion luminescence mechanism, (a) electrons transition, (b) cross relaxation of electrons occurs between the two ions, (c) based on cross relaxation, emitting multiple photons and releasing luminescence, (d) electrons transition and transferring energy.

Upconversion/downconversion emission has been applied in various fields, such as biological imaging, lasers, 3D displays, lighting, anti-counterfeiting, and so on. In order to enhance emission ability, relevant studies have been reported. The following will briefly introduce several common enhancement methods.

### 3. Luminescence Emission Regulation Pathway

#### 3.1. Regulation of Local Crystal Fields

The f-f transitions of trivalent rare earth ions are mostly caused by electric dipole interactions. Due to the asymmetric crystal field, the opposite parity is mixed into a 4f configuration and the transition prohibition can be broken to a certain extent. The mismatch between cation radius and valence state can effectively regulate the local crystal field, which is more beneficial in enhancing the radiation and absorption transition probability of rare earth ions, which then affect the upconversion/downconversion luminescence [49–51].

By doping some metal ions to regulate the local crystal field, or introducing different rare earth ions, the crystal phase will be transformed, and diverse upconversion emission can be achieved. As shown in Figure 5, multicolor and multimode luminescent modulations are successfully obtained in the  $\text{Tb}^{3+}/\text{Eu}^{3+}$  co-doped  $(\text{K}_{0.5}\text{Na}_{0.5})\text{NbO}_3$  system. The phase transition is caused by the subtle difference of  $\text{Tb}^{3+}/\text{Eu}^{3+}$  radius and charge imbalance. Combining with energy transfer engineering,  $(\text{K}_{0.5}\text{Na}_{0.5})\text{NbO}_3:\text{Tb}^{3+}, \text{Eu}^{3+}$  obtains intense green and red multimodal emission.

#### 3.2. Structure Design

In the process of crystal particle growth, the surface will be affected by functional groups in the reaction solution, resulting in fluorescence quenching of activator ions. In order to protect the activator ions from external interference, a shell layer is grown on the surface of the core layer through the design of a core-shell structure.

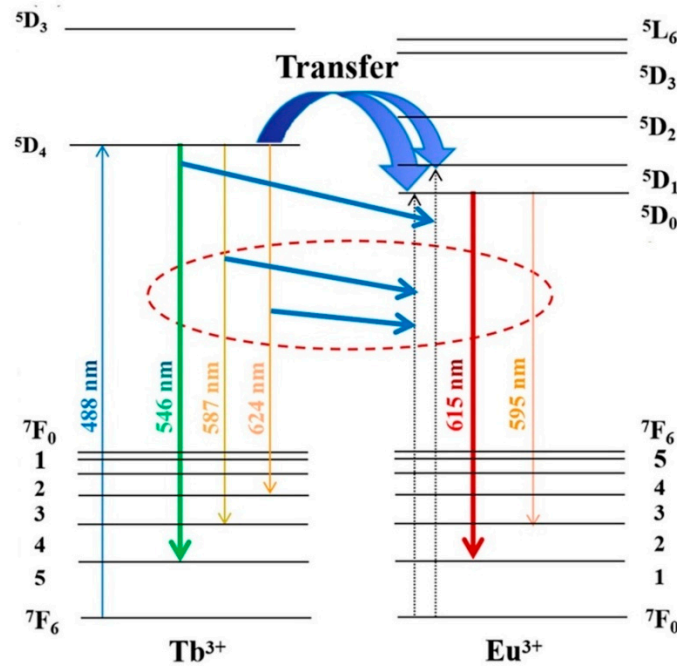


Figure 5. The energy transfer and luminescence emission process of  $(K_{0.5}Na_{0.5})NbO_3:Tb^{3+}, Eu^{3+}$ . Reprinted with permission from Ref. [52]. Copyright 2021 Elsevier Publishing Group.

The construction of the core-shell structure allows for the spatial separation of activators and downconversion centers, greatly suppressing adverse cross-relaxation processes [53–55]. As shown in Figure 6,  $Ce^{3+}$  is introduced into the inner core, which serves the regulation of upconversion emission and facilitates ultraviolet photon harvesting with a subsequent energy transfer to downshifting activators in the outer shell layer.

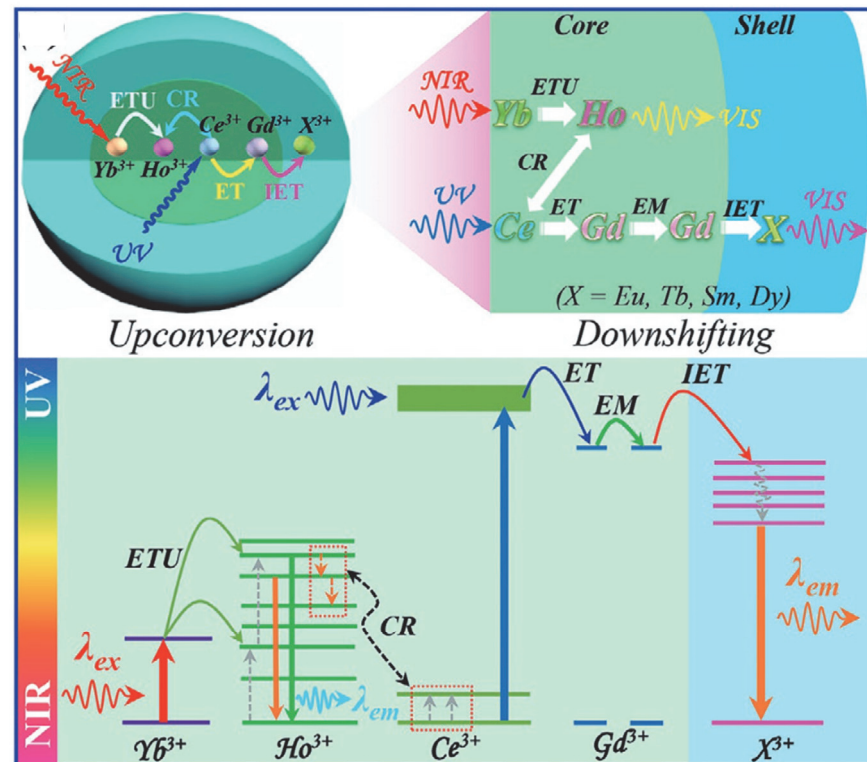
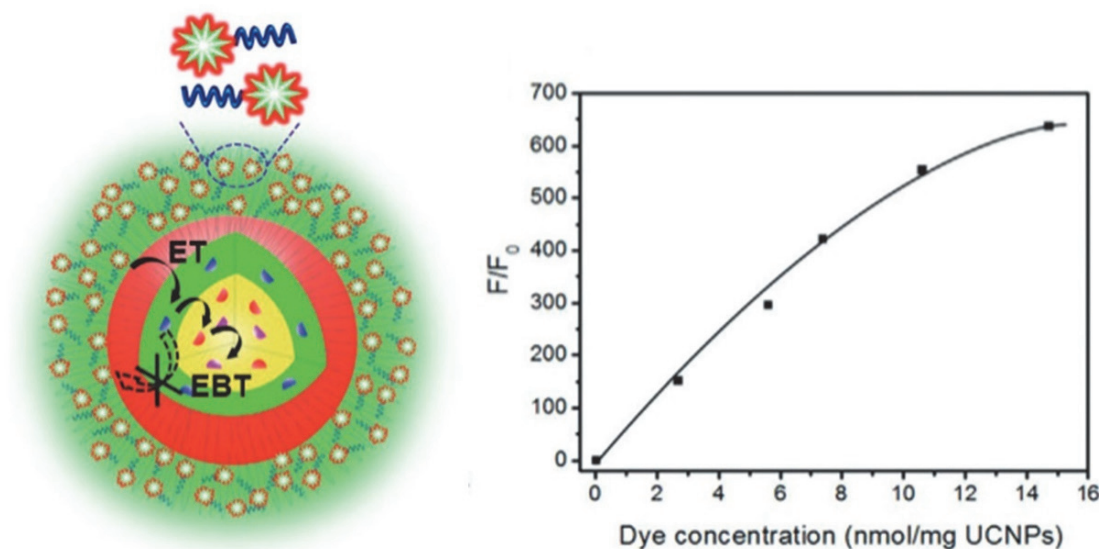


Figure 6. Schematic design of core-shell nanostructure for achieving  $Ce^{3+}$ -induced tunable dual-mode emission. Reprinted with permission from Ref. [56]. Copyright 2020 Wiley Publishing Group.

### 3.3. Dye Sensitized Upconversion

It is common to enhance the upconversion luminescence of activator ions by using  $\text{Yb}^{3+}$  as a sensitizer, but the absorption cross section of organic dye molecules is wider, which can better enhance the energy absorption of activator ions. Organic dyes are used as ligands to transfer the energy absorbed by dye molecules to rare earth ions through molecular design and fluorescence resonance energy transfer process [57,58]. As shown in Figure 7, when Alk-pi dye is used to modify upconversion particles, the blue shift emission of Alk-pi overlaps with the  $\text{Nd}^{3+}$  absorption spectrum, which obtains a sensitization effect and significant luminescence enhancement.



**Figure 7.** Schematic illustration of Alk-pi dye and  $\text{Nd}^{3+}$  with upconversion emission enhancement at various concentrations of Alk-pi. Reprinted with permission from Ref. [59]. Copyright 2020 Wiley Publishing Group.

## 4. Synthetic Methods

At present, the liquid phase method and solid phase method are the main ways to synthesize rare earth luminescent materials with excellent properties. Solid phase synthesis is simple and easy to operate, but the size and morphology of the product are not uniform. Compared with the solid phase method, the liquid phase method not only has the characteristics of simple synthesis and convenient operation, but also has the advantages of mild reaction conditions, controllable particle size and morphology of products, high product purity, fewer surface defects, and is suitable for the preparation of various materials. Specific preparation methods include the high temperature solid phase method, low temperature combustion method, hydrothermal method, microemulsion method, coprecipitation method, sol-gel method, and so on.

The hydrothermal method is commonly used for the preparation of rare earth luminescent materials. DI water is the main reaction environment. The growth of luminescent nanocrystals is influenced by adjusting reaction temperature, pressure, surfactants, and other conditions. As shown in Figure 8, the crystal phase structure of  $(\text{Y}_{0.95}\text{Eu}_{0.05})\text{PO}_4$  can be transformed from h- to t- by changing the pH, and the adjustment of crystal structure induces an increase in luminescent emission intensity. In addition, the obtained crystal morphology is uniform and the size is controllable.

The thermal decomposition method generally requires a reaction to satisfy anaerobic and anhydrous conditions. The reaction can be added into a certain amount of oleic acid and octadecene to control the morphology, size, and dispersion of the product. The final sample is obtained under a two-step temperature control. Wu et al. obtained multiple morphologies of  $\text{NaGdF}_4:\text{Yb}^{3+}$ ,  $\text{Tm}^{3+}@\text{NaGdF}_4$  rare earth luminescent materials by thermal decomposition method, as shown in Figure 9. By changing the molar ratio of the precursor

core to the shell and heating rate, the spherical, hexagonal planar, tetrahedral, and floral morphologies of 15–100 nm were obtained.

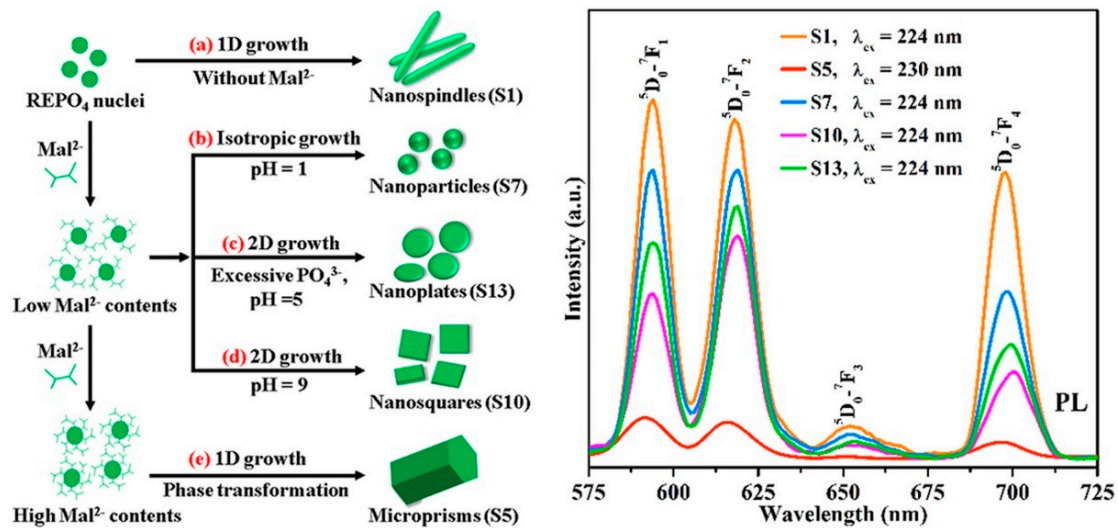


**Figure 8.** Schematic illustration of the possible formation mechanisms of samples and photoluminescence emission spectrum. Reprinted with permission from Ref. [60]. Copyright 2021 Elsevier Publishing Group.

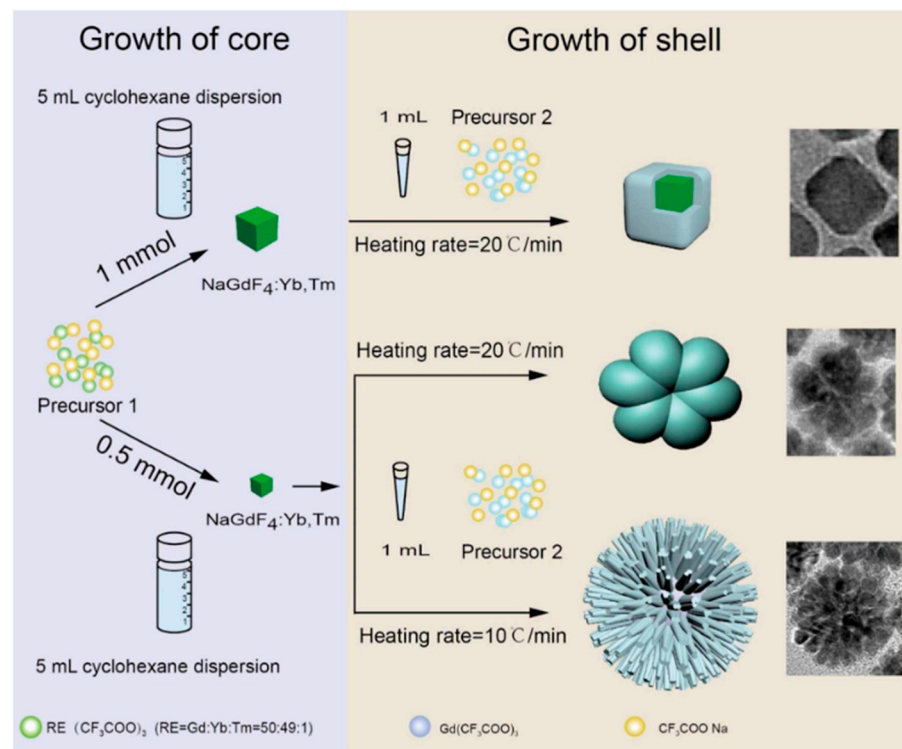


**Figure 9.** Thermal decomposition synthesis of NaGdF<sub>4</sub>:Yb<sup>3+</sup>, Tm<sup>3+</sup>@NaGdF<sub>4</sub>. Reprinted with permission from Ref. [61]. Copyright 2017 Royal Society of Chemistry.

The sol-gel method is based on some chemically active components such as metal complexes and esters as precursors, which then hydrolyze and condense. By controlling the pH, reaction temperature and other conditions, colloids of different shapes are formed. After further aging, the reticular gel is obtained, and finally, the product is obtained through drying, calcination, and other steps. Hediger prepared Y<sub>3</sub>TaO<sub>7</sub>:x% Eu<sup>3+</sup> rare earth luminescent material by the sol-gel method [62]. A solution was first prepared with

2-ethoxyethanol, tantalum ethoxide,  $Y(NO_3)_3$ , and  $Eu(NO_3)_3$ . An amount of 10 mL of  $NH_4OH$  ethanol solution was added into the above mixture and continuously stirred for 1 h. The resulting solid was separated by centrifugation. Finally, the obtained solid was annealed at 900 °C or 1100 °C.

The coprecipitation method is to form precipitate, and add the precipitant to a soluble solution containing cations. Subsequently, the precipitate is washed and dried to obtain the target product. Meenambal used the coprecipitation method to prepare  $\beta-Ca_3(PO_4)_2:Gd^{3+}, Dy^{3+}, Yb^{3+}$  rare earth luminescent materials [63]. The prepared  $(NH_4)_2HPO_4$  aqueous solution was dropwise added to a cationic nitrate solution containing  $Ca^{2+}, Gd^{3+}, Dy^{3+}$ , and  $Yb^{3+}$  at 90 °C. After the solution mixture was dissolved, a white precipitate was gradually formed based on the addition of  $NH_4OH$  at a pH of ~8. The suspension was stirred at 90 °C for 3 h with the appearance of precipitate and dried overnight at 120 °C.

High temperature solid-phase synthesis is the process of crystal growth between solid interfaces at high temperature (1000~1500 °C) to generate a large number of composite oxides. The high temperature solid-phase method is a traditional powder synthesis process, which has some characteristics such as high energy consumption, insufficient powder size, and easy mixing of impurities. However, the powder particles prepared by this method have no agglomeration, and have a good filling ability, low cost, and simple preparation process. An et al. prepared color-tunable  $Ca_{20}Al_{26}Mg_3Si_3O_{68}:Ce^{3+}, Tb^{3+}$  phosphors via the high temperature solid-phase method. The oxide raw materials were thoroughly ground and placed in a crucible for high-temperature sintering under a reducing gas mixture of 10%  $H_2$ /90%  $N_2$  at 1350 °C for 2 h [64]. Finally, well-crystallized phosphor was obtained.

## 5. Anti-Counterfeiting Application

The rapid development of modern technology and the inundation of counterfeit products have promoted the emergence of various anti-counterfeiting technologies. Anti-counterfeiting technology is closely linked to many disciplines and has also become the crystallization of the combination and comprehensive application of multidisciplinary scientific and technological achievements, such as holograms, plasmons, and communication encryption [65–68]. Rare earth luminescent materials have the advantages of good visibility and diverse colors, and can become ideal anti-counterfeiting and information encryption materials.

Optical patterns, as a highly promising protection symbol, are often used for high security protection of valuable documents or items. However, the display of high spatial resolution patterns is particularly crucial in the use of luminescent materials. Rare earth doped luminescent materials exhibit better characteristics in emission profile, fluorescence decay time, photochemical stability, and self-fluorescence background signal.

A good method has been provided for designing practical high-capacity luminescent patterns and encoding by precisely manipulating the polychromatic output and continuously tuning the decay lifetime of nanostructures. Based on the multi-layer  $NaGdF_4$  core-shell structure, the shell is changed by  $Nd^{3+}, Tm^{3+}, Er^{3+}$ , and the conversion of green and blue luminescence is achieved under excitation at 796 nm and 980 nm [69].

As shown in Figure 10a, time-gated luminescence demonstrates lifetime multiplexing. The delay time is set by a combination of pulse synchronizers and choppers to filter out faster attenuated luminescence. The SMILES pattern is used for encoding and decoding together with time-gated luminescence (Figure 10b). The experimental results are shown in the upper part. Steady-state luminescence of SMILE was observed at 980 nm irradiation. However, no signal can be picked up by time-gated mode or 808 nm irradiation. Then, multiple  $Tm@Tb@Y@Er@Nd@Y$  nanoparticles were added to encode MILES. In the time-gated mode, the short-life signal SMILE is filtered, while the long-life MILES emitted by  $Tb^{3+}$  is detected. The same pattern can be seen at 808 nm excitation.

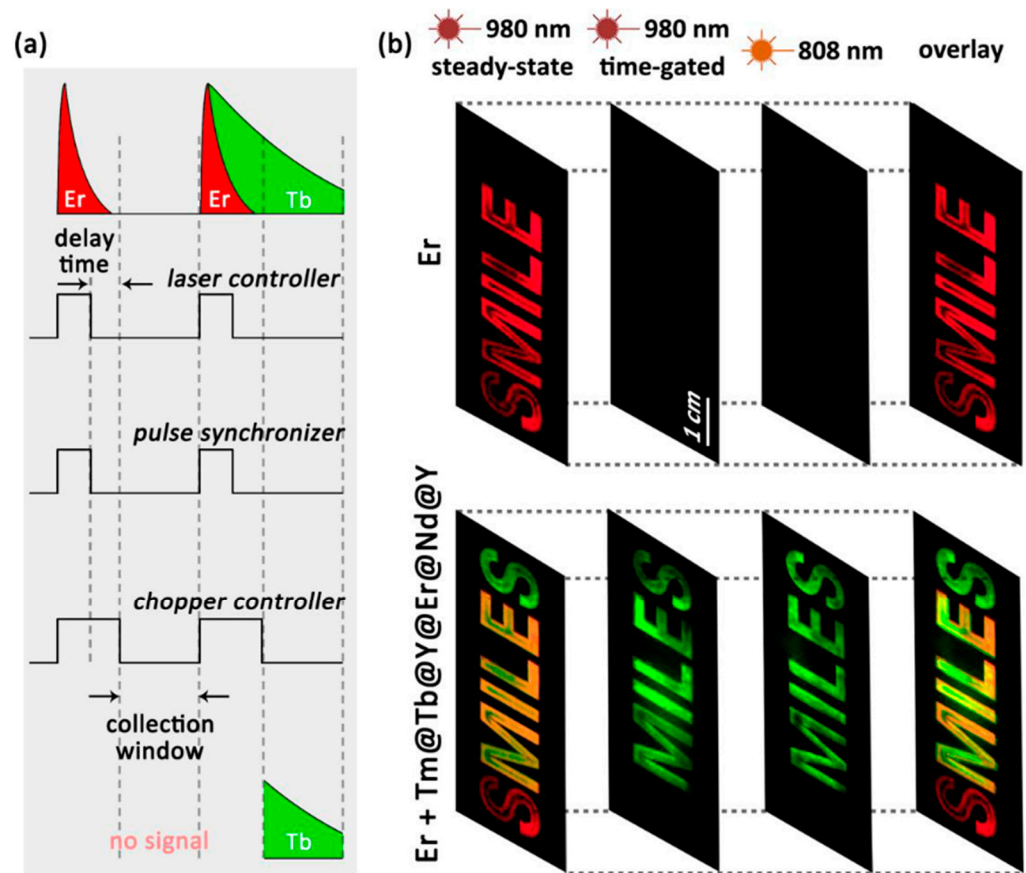


**Figure 10.** (a) Lifetime multiplexing is used for anti-counterfeiting by time-gated technology, (b) luminescent signal pattern. Reprinted with permission from Ref. [70]. Copyright 2017 American Chemical Society.

The photoresponsive supermolecule coordination polyelectrolyte (SCP) is constructed by metal coordination and ion interaction. Förster resonance energy transfer promotes photochromism of rare earth ions and diarylenes. The closed-loop/open-loop isomerization of diarylene units leads to the photoreversible light-emitting switch of SCP. Anti-counterfeiting ink is prepared based on SCP and pattern printing, presenting multiple information patterns under UV and visible light radiation, as shown in Figure 11.

The interaction between materials to achieve efficient luminescence performance is also constantly being explored.  $\text{NaYF}_4:\text{Yb}/\text{Tm}@/\text{NaYF}_4:\text{Yb}$  serves as a core layer and grows ultra small  $\text{CsPbX}_3$  ( $X = \text{Cl}, \text{Br}$ ) quantum dots, achieving polychromatic downconversion luminescence and visible light excitation upconversion luminescence, as shown in Figure 12. Under the action of polystyrene, a multicolor fluorescent anti-counterfeiting ink with strong stability is obtained.

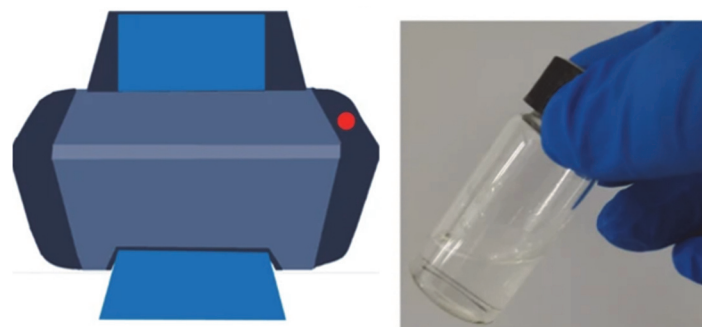


**Figure 11.** Cont.

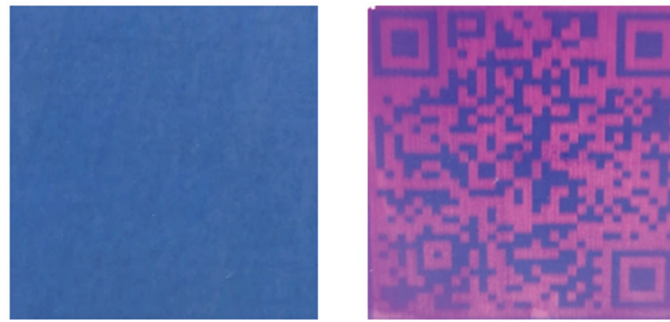


**Figure 11.** Pattern printing using SCP as the ink. Reprinted with permission from Ref. [71]. Copyright 2021 Nature Publishing Group.

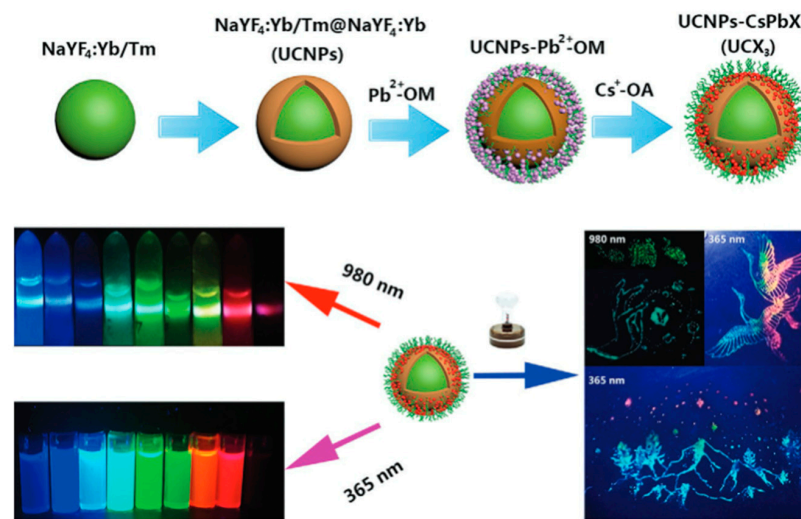


**Figure 12.** Multicolor fluorescent anti-counterfeiting ink based on NaYF<sub>4</sub>:Yb/Tm@NaYF<sub>4</sub>:Yb and CsPbX<sub>3</sub> (X = Cl, Br). Reprinted with permission from Ref. [72]. Copyright 2021 Elsevier Publishing Group.

Based on ions exchange strategy, a multimodal nanocomposite composed of rare earth doped upconversion nanoparticles and EuSe semiconductors is obtained, and achieves blue and white light emission. At the same time, the content of Tb<sup>3+</sup> in the upconversion nanoparticles is changed, and time-gated technology is used to filter Tb<sup>3+</sup> or Eu<sup>3+</sup> long-lived upconversion emission, expanding the modulation of luminescent colors and achieving the loading of optical information, as shown in Figure 13.

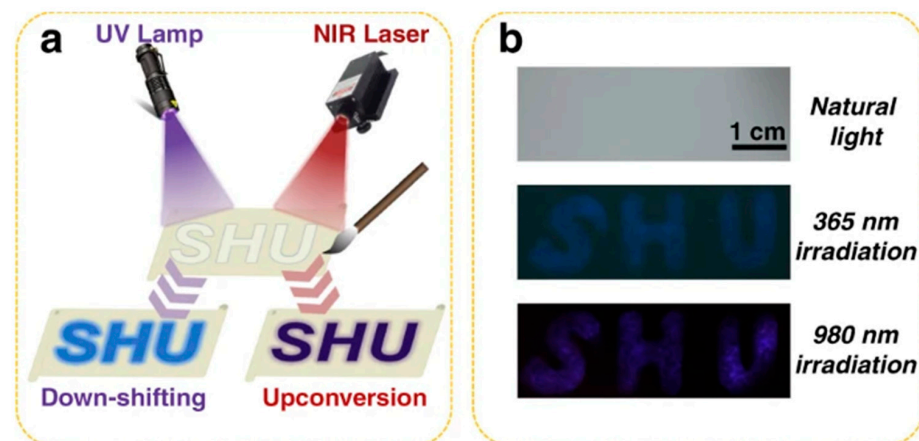


**Figure 13.** (a) “SHU” pattern with different laser excitation, (b) color change display diagram. Reprinted with permission from Ref. [73]. Copyright 2022 Nature Publishing Group.

X-ray or UV photo charge storage phosphors have been developed in anti-counterfeiting and information storage. By doping  $\text{Bi}^{3+}$  and  $\text{Ln}^{3+}$  ( $\text{Ln} = \text{Tb}, \text{Pr}, \text{or Dy}$ ) into  $\text{LiLuGeO}_4$ , the process of carrier capture and release is adjusted to achieve energy transfer. Meanwhile, the doping concentration is controlled under 303 K to 650 K, and the fluorescent powder can achieve high TL intensity to obtain an afterglow of over 10 or 40 h under X-ray or ultraviolet excitation, which has been used in information storage and anti-counterfeiting [74].

The proportion of doped ions can be adjusted, and a controllable hexagonal  $\text{NaYF}_4:\text{Yb}^{3+}/\text{Ho}^{3+}/\text{Ce}^{3+}$  microcrystal is obtained. Cross relaxation and electron population redistribution occur between  $\text{Ho}^{3+}$  and  $\text{Ce}^{3+}$ . In the temperature range of 300–500 K, the ratio of red to green radiant intensity (IR/IG), as the independent variable of temperature, has good linear characteristics. Meanwhile, potential applications have been obtained for anti-counterfeiting based on the light response generated by temperature changes [75].

The anti-counterfeiting encryption of optical information has gradually been developed through the structural design of materials. Layered hydroxides and rare earth ions are assembled layer by layer, and combined with pyromellitic acid, rare earth ion doped information encryption material is obtained. Under the excitation of ultraviolet and visible light, layered hydroxides doped with rare earth ions exhibit different color emissions, as shown in Figure 14. Combined with symmetric and asymmetric algorithms, multi-dimensional advanced information encryption is achieved.

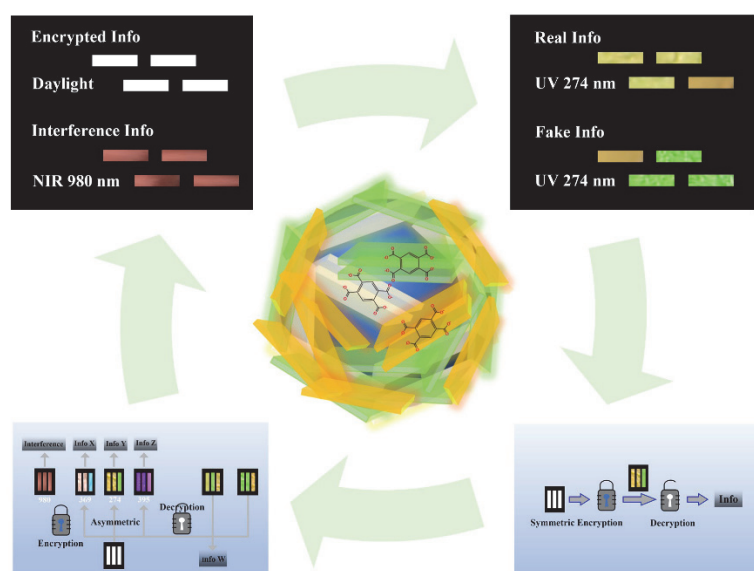


**Figure 14.** Programmable broadband responsive lanthanide-doped nanoarchitecture for information encryption. Reprinted with permission from Ref. [76]. Copyright 2022 Wiley Publishing Group.

Zhang et al. [77] used  $\text{Na}_2\text{CaGe}_2\text{O}_6:\text{Tb}^{3+}$  phosphor to prepare anti-counterfeiting ink and attached it to a fixed substrate to obtain anti-counterfeiting patterns. Under light irradiation at 254 nm,  $\text{Na}_2\text{CaGe}_2\text{O}_6:\text{Tb}^{3+}$  can achieve multicolor transformation based on trap depth and phonon-assisted cross relaxation. Tian et al. [78] synthesized multicolor  $\text{LiTaO}_3:\text{Pr}^{3+}$  phosphor with different doping concentrations of  $\text{Pr}^{3+}$  ions, and obtained a multicolor anti-counterfeiting device. Depending on the color difference and duration, the prepared anti-counterfeiting device displayed four different photoluminescence colors under 254 nm ultraviolet light and was applied to a two-dimensional code display. Zhang et al. [79] prepared multifunctional  $\text{NaNbO}_3:\text{Pr}^{3+}, \text{Er}^{3+}$  phosphor and embedded them into polymer films to obtain multimodal luminescence (including multiple stimulus responses and up/downconversion luminescence emission). This film is used in the construction of optical anti-counterfeiting security.

## 6. Conclusions and Perspective

The research of anti-counterfeiting technology based on luminescent materials has gradually become an important subject in the field of optical anti-counterfeiting. Rare earth luminescent materials have been used as the most important components in anti-counterfeiting, showing good optical properties such as upconversion and downconversion. Furthermore, the tuning of light output can be achieved through regulation of local crystal fields, structural design, and dye sensitization methods. Meanwhile, the electron transition process can be determined to obtain the optimal energy path based on the analysis of the up/downconversion luminescent emission mechanism. According to the reaction conditions and functional requirement, the preparation of rare earth doped materials can be carried out through the selection of methods, such as hydrothermal method, thermal decomposition method, sol-gel, and coprecipitation method. Anti-counterfeiting technology is closely linked to many disciplines and is also the crystallization of the combination and comprehensive application of multidisciplinary scientific and technological achievements. Rare earth ions doped luminescent materials possess better characteristics in emission profile, fluorescence decay time, and photochemical stability, which achieve polychromatic output and multiple excitation wavelength recognition. Anti-counterfeiting ink is prepared and patterns printed, presenting multiple information patterns under UV and visible light radiation. Time-gated technology is used to filter  $Tb^{3+}$  or  $Eu^{3+}$  long-lived upconversion emission, expanding the modulation of luminescent colors and achieving the loading of optical information. The excitation source also affects the generation of optical patterns, achieving anti-counterfeiting function. The reaction conditions and cross relaxation also alter the light output, resulting in multiple anti-counterfeiting. Combined with the use of algorithms, the luminescence of rare earth doped materials has also been further analyzed, obtaining multi-dimensional encryption and anti-counterfeiting.

In the more recent development of rare earth luminescent materials, mode supplementation has been achieved through crystal modification, ligand assistance, lattice occupation, or by combination with other optical materials. Ion co-doping strategy and different substrates are coordinated, such as oxides, fluorides,  $Eu^{3+}$  and  $Eu^{2+}$ . In addition, the concentration of doped ions can be operated to adjust the trap depth and achieve color emission duration tuning. Moreover, the bandgap of substrate is also an important factor affecting luminescence. The lattice occupation of ions is optimized to maximize the luminescence effect. In the light output mode, multimodal anti-counterfeiting devices can be designed by combining forms such as photoluminescence, electroluminescence, and thermally excited luminescence, for manipulation.

The development of multimodal anti-counterfeiting materials is promotive to achieve variable excitation mode, multicolor luminescence, dynamic luminescence, adjustable luminescence color, and multimodal luminescence. The excitation mode or power is changed to produce visually recognizable color changes, not only dynamic optical information changes generated in the spatial dimension, achieving not only high-level security and anti-counterfeiting, but also high-capacity and multi-scene information storage.

Overall, this mini review aims to provide a simple summary and discussion on up/downconversion luminescence and its anti-counterfeiting application in rare earth doped luminescent materials. There is still much room for basic research, as well as further exploration of new strategies for diverse applications. In the near future, multidisciplinary collaborative research will continue to drive the development of this field.

**Author Contributions:** Conceptualization, Z.C. and H.Z. (Hang Zhu); writing—original draft preparation, Z.C., H.Z. (Hang Zhu), J.Q., Z.L. and X.H.; writing—review and editing, Z.C., H.Z. (Hang Zhu), J.Q., Z.L., X.H., Y.G., Y.F., H.Z. (Huazhong Zhu), W.N., Z.Y., D.L. and L.Z. All authors have read and agreed to the published version of the manuscript.

**Funding:** This research was funded by scientific research project of Huzhou College (2023HXKM02).

**Institutional Review Board Statement:** Not applicable.

**Informed Consent Statement:** Not applicable.

**Data Availability Statement:** Not applicable.

**Conflicts of Interest:** The authors declare no conflict of interest.

## References

1. Yan, C.L.; Zhao, H.G.; Perepichka, D.F.; Rosei, F. Lanthanide ion doped upconverting nanoparticles: Synthesis, structure and properties. *Small* **2016**, *12*, 3888–3907. [[CrossRef](#)] [[PubMed](#)]
2. Zhang, H.X.; Chen, Z.H.; Liu, X.; Zhang, F. A mini-review on recent progress of new sensitizers for luminescence of lanthanide doped nanomaterials. *Nano Res.* **2020**, *13*, 1795–1809. [[CrossRef](#)]
3. Sutter, J.P.; Béreau, V.; Jubault, V.; Bretosh, K.; Pichon, C.; Duhayon, C. Magnetic anisotropy of transition metal and lanthanide ions in pentagonal bipyramidal geometry. *Chem. Soc. Rev.* **2022**, *51*, 3280–3313. [[CrossRef](#)]
4. Zhou, B.; Tao, L.L.; Chai, Y.; Lau, S.P.; Zhang, Q.Y.; Tsang, Y.H. Constructing interfacial energy transfer for photon up- and down-conversion from lanthanides in a core-shell nanostructure. *Angew. Chem. Int. Ed.* **2016**, *55*, 12356–12360. [[CrossRef](#)] [[PubMed](#)]
5. Dong, H.; Sun, L.D.; Yan, C.H. Energy transfer in lanthanide upconversion studies for extended optical applications. *Chem. Soc. Rev.* **2015**, *44*, 1608–1634. [[CrossRef](#)]
6. Liang, L.L.; Feng, Z.W.; Zhang, Q.M.; Cong, T.D.; Wang, Y.; Qin, X.; Yi, Z.G.; Ang, M.J.Y.; Zhou, L.; Feng, H.; et al. Continuous-wave near-infrared stimulated-emission depletion microscopy using downshifting lanthanide nanoparticles. *Nat. Nanotechnol.* **2021**, *16*, 975–980. [[CrossRef](#)]
7. Jiang, Z.; He, L.R.; Yang, Z.W.; Qiu, H.B.; Chen, X.Y.; Yu, X.J.; Li, W.W. Ultra-wideband-responsive photon conversion through co-sensitization in lanthanide nanocrystals. *Nat Commun.* **2023**, *14*, 827. [[CrossRef](#)]
8. Dwivedi, A.; Singh, A.K.; Singh, S.K. Wide-bandgap lanthanide niobates: Optical properties and applications. *Mater. Res. Bull.* **2020**, *131*, 110960. [[CrossRef](#)]
9. Ma, Q.M.; Zhang, M.; Yao, C.; Du, Y.P.; Yang, D.Y. Supramolecular hydrogel with luminescence tunability and responsiveness based on co-doped lanthanide and deoxyguanosine complex. *Chem. Eng. J.* **2020**, *394*, 124894. [[CrossRef](#)]
10. Lyu, T.S.; Dorenbos, P.; Wei, Z.H. Designing LiTaO<sub>3</sub>:Ln<sup>3+</sup>, Eu<sup>3+</sup> (Ln = Tb or Pr) perovskite dosimeter with excellent charge carrier storage capacity and stability for anti-counterfeiting and flexible X-ray imaging. *Chem. Eng. J.* **2023**, *461*, 141685. [[CrossRef](#)]
11. Li, H.; Wang, X.; Li, X.L.; Zeng, S.J.; Chen, G.Y. Clearable shortwave-infrared-emitting NaErF<sub>4</sub> nanoparticles for noninvasive dynamic vascular imaging. *Chem. Mater.* **2020**, *32*, 3365–3375. [[CrossRef](#)]
12. Zhang, G.D.; Dang, P.P.; Lian, H.Z.; Huang, S.S.; Yang, W.; Cheng, Z.Y.; Lin, J. Tailoring the highly efficient upconversion luminescence of all-inorganic Er<sup>3+</sup>-based halide double perovskites by introducing various energy trapping centers. *Adv. Opt. Mater.* **2022**, *10*, 2201220. [[CrossRef](#)]
13. Liu, X.M.; Li, R.H.; Xu, X.L.; Jiang, Y.Y.; Zhu, W.J.; Yao, Y.; Li, F.Y.; Tao, X.F.; Liu, S.J.; Huang, W.; et al. Lanthanide(III)-Cu<sub>4</sub>I<sub>4</sub> organic framework scintillators sensitized by cluster-based antenna for high-resolution X-ray imaging. *Adv. Mater.* **2023**, *35*, 2206741. [[CrossRef](#)] [[PubMed](#)]
14. Wang, Y.; Zheng, K.Z.; Song, S.Y.; Fan, D.Y.; Zhang, H.J.; Liu, X.G. Remote manipulation of upconversion luminescence. *Chem. Soc. Rev.* **2018**, *47*, 6473–6485. [[CrossRef](#)]
15. Wu, S.L.; Xia, H.B.; Xu, J.H.; Sun, X.Q.; Liu, X.G. Manipulating luminescence of light emitters by photonic crystals. *Adv. Mater.* **2018**, *30*, 1803362. [[CrossRef](#)]
16. Vahedigharehchopogh, N.; Kibrıslı, O.; Erol, E.; Çelıkbilek Ersundu, M. A straightforward approach for high-end anti-counterfeiting applications based on NIR laser-driven lanthanide doped luminescent glasses. *J. Mater. Chem. C* **2021**, *9*, 2037–2046. [[CrossRef](#)]
17. Liu, S.B.; Yan, L.; Li, Q.Q.; Huang, J.S. Tri-channel photon emission of lanthanides in lithium-sublattice core-shell nanostructures for multiple anti-counterfeiting. *Chem. Eng. J.* **2020**, *397*, 125451. [[CrossRef](#)]
18. Li, X.; Chen, H.; Kirillov, A.M.; Xie, Y.J.; Shan, C.F.; Wang, B.K.; Shi, C.L. A paper-based lanthanide smart device for acid-base vapour detection, anti-counterfeiting and logic operations. *Inorg. Chem. Front.* **2016**, *3*, 1014–1020. [[CrossRef](#)]
19. Zhao, S.C.; Gao, M.; Li, J.F. Lanthanides-based luminescent hydrogels applied as luminescent inks for anti-counterfeiting. *J. Lumin.* **2021**, *236*, 118128. [[CrossRef](#)]
20. Ataei, P.; Staegemann, D. Application of microservices patterns to big data systems. *J. Big Data* **2023**, *10*, 56. [[CrossRef](#)]
21. Liu, Y.Z.; Liang, S.F.; Yuan, C.R.; Best, A.; Kappl, M.; Koynov, K.; Butt, H.; Wu, S. Fabrication of anticounterfeiting nanocomposites with multiple security features via integration of a photoresponsive polymer and upconverting nanoparticles. *Adv. Funct. Mater.* **2021**, *31*, 2103908. [[CrossRef](#)]
22. Abdollahi, A.B.; Nikzaban, G.S.; Sardari, N.; Jorjeisi, S.; Dashti, A. Dual-Color photoluminescent functionalized nanoparticles for static-dynamic anticounterfeiting and encryption: First collaboration of spiropyran and coumarin. *ACS Appl. Mater. Interfaces* **2023**, *15*, 7466–7484. [[CrossRef](#)] [[PubMed](#)]
23. Bian, F.K.; Sun, L.Y.; Chen, H.X.; Wang, Y.; Wang, L.; Shang, L.R.; Zhao, Y.J. Bioinspired perovskite nanocrystals-integrated photonic crystal microsphere arrays for information security. *Adv. Sci.* **2022**, *9*, 2105278. [[CrossRef](#)]

24. Zhao, S.S.; Li, G.G.; Guo, Q.; Wang, Y.X.; Zhang, M.J.; Zhou, Y.J.; Jin, S.; Zhu, M.Z.; Zhuang, T.T. Visualizing circularly polarized long afterglow for information security. *Adv. Opt. Mater.* **2023**, *11*, 2202933. [[CrossRef](#)]
25. Liu, M.L.; Wu, Q.; Shi, H.F.; An, Z.F.; Huang, W. Progress of research on organic/organometallic mechanoluminescent materials. *Acta Chim. Sin.* **2018**, *76*, 246–258. [[CrossRef](#)]
26. Gu, M.; Zhang, Q.M.; Lamon, S. Nanomaterials for optical data storage. *Nat. Rev. Mater.* **2016**, *1*, 16070. [[CrossRef](#)]
27. Sun, N.F.; Chen, Z.Y.; Wang, Y.K.; Wang, S.; Xie, Y.; Liu, Q. Random fractal-enabled physical unclonable functions with dynamic AI authentication. *Nat. Commun.* **2023**, *14*, 2185. [[CrossRef](#)]
28. Deng, Z.M.; Li, L.L.; Tang, P.P.; Jiao, C.Y.; Yu, Z.Z.; Koo, C.M.; Zhang, H.B. Controllable surface-grafted MXene inks for electromagnetic wave modulation and infrared anti-counterfeiting applications. *ACS Nano* **2022**, *16*, 16976–16986. [[CrossRef](#)]
29. Wan, W.; Han, X.X.; Zhou, Y.Y.; Chen, F.R.; Jing, X.P.; Ye, S. Constructing perovskite-like oxide CsCa<sub>2</sub>Ta<sub>3</sub>O<sub>10</sub>: Yb, Er@Cs(Pb<sub>x</sub>Mn<sub>1-x</sub>)(Cl<sub>y</sub>Br<sub>1-y</sub>)<sub>3</sub> perovskite halide composites for five-dimensional anti-counterfeiting barcodes applications. *Chem. Eng. J.* **2021**, *409*, 128165. [[CrossRef](#)]
30. Wang, J.X.; Li, P.Y.; Ji, C.D.; Wu, J.H.; Fan, M.Y.; Guan, J.; Yin, M.Z. A dually responsive cyanostilbene derivative for paper fluorescence anti-counterfeiting and informational encryption. *J. Mater. Chem. C* **2022**, *10*, 15145–15151. [[CrossRef](#)]
31. Xu, R.; Feng, M.; Chen, Z.Y.; Yang, J.X.; Han, D.D.; Xie, J.Y.; Song, F. Non-uniform angular spectrum method in a complex medium based on iteration. *Opt. Lett.* **2022**, *47*, 1972–1975. [[CrossRef](#)] [[PubMed](#)]
32. Liu, Y.; Chen, W.H.; Li, L.H.; Yang, B. Si-assisted N, P co-doped room temperature phosphorescent carbonized polymer dots: Information encryption, graphic anti-counterfeiting and biological imaging. *J. Colloid Interface Sci.* **2022**, *609*, 279–288. [[CrossRef](#)] [[PubMed](#)]
33. Terranova, S.; Costa, F.; Manara, G.; Genoves, S. Three-dimensional chipless RFID tags: Fabrication through additive manufacturing. *Sensors* **2020**, *20*, 4740. [[CrossRef](#)]
34. Wang, J.J.; Li, Y.J.; Wang, T.H.; He, F.Y.; Yin, Z.Y.; Qiu, J.B.; Song, Z.G. Internal electric field and oxygen vacancies synergistically enhancing luminescence properties of Eu<sup>3+</sup>-doped bismuth oxychloride microcrystals. *J. Lumin.* **2021**, *240*, 11845. [[CrossRef](#)]
35. Liao, J.S.; Han, Z.; Lin, F.L.; Fu, B.; Gong, G.L.; Yan, H.K.; Hang, H.P.; Wen, H.R.; Qiu, B. Simultaneous thermal enhancement of upconversion and downshifting luminescence by negative thermal expansion in nonhygroscopic ZrSc(WO<sub>4</sub>)<sub>2</sub>PO<sub>4</sub>:Yb/Er phosphors. *Inorg. Chem.* **2023**, *62*, 9518–9527. [[CrossRef](#)]
36. Liao, J.S.; Wang, M.H.; Lin, F.L.; Han, Z.; Fu, B.; Tu, D.T.; Chen, X.Y.; Qiu, B.; Wen, H.R. Thermally boosted upconversion and downshifting luminescence in Sc<sub>2</sub>(MoO<sub>4</sub>)<sub>3</sub>:Yb/Er with two-dimensional negative thermal expansion. *Nat. Commun.* **2022**, *13*, 2090. [[CrossRef](#)]
37. Li, L.P.; Li, T.Y.; Hu, Y.; Cai, C.Y.; Li, Y.Q.; Zhang, X.F.; Liang, B.L.; Yang, Y.M.; Qiu, J.R. Mechanism of the trivalent lanthanides' persistent luminescence in wide bandgap materials. *Light-Sci. Appl.* **2022**, *11*, 51. [[CrossRef](#)]
38. Zhou, J.J.; Leañó, L.J.; Liu, Z.Y.; Jin, D.Y.; Wong, K.L.; Liu, R.S.; Bünzli, J.G. Impact of lanthanide nanomaterials on photonic devices and smart applications. *Small* **2018**, *14*, 1801882. [[CrossRef](#)]
39. Ward, M.D. Mechanisms of sensitization of lanthanide (III)-based luminescence in transition metal/lanthanide and anthracene/lanthanide dyads. *Coordin. Chem. Rev.* **2010**, *254*, 2634–2642. [[CrossRef](#)]
40. Auzel, F. Upconversion and anti-stokes processes with f and d ions in solids. *Chem. Rev.* **2004**, *104*, 139–173. [[CrossRef](#)]
41. Rathaiyah, M.; Haritha, P.; Linganna, K.; Monteseuro, V.; Martín, I.R.; Lozano-Gorrín, A.D.; Babu, P.; Jayasankar, C.K.; Lavín, V.; Venkatramu, V. Infrared-to-visible light conversion in Er<sup>3+</sup>-Yb<sup>3+</sup>:Lu<sub>3</sub>Ga<sub>5</sub>O<sub>12</sub> nanogarnets. *ChemPhysChem* **2015**, *16*, 3928–3936. [[CrossRef](#)]
42. Rathaiyah, M.; Haritha, P.; Lozano-Gorrín, A.D.; Babu, P.; Jayasankar, C.K.; Rodríguez-Mendoza, U.R.; Lavín, V.; Venkatramu, V. Stokes and anti-stokes luminescence in Tm<sup>3+</sup>/Yb<sup>3+</sup>-doped Lu<sub>3</sub>Ga<sub>5</sub>O<sub>12</sub> nano-garnets: A study of multipolar interactions and energy transfer dynamics. *Phys. Chem. Chem. Phys.* **2016**, *18*, 14720–14729. [[CrossRef](#)] [[PubMed](#)]
43. Marin, R.; Jaque, D.; Benayas, A. Switching to the brighter lane: Pathways to boost the absorption of lanthanide-doped nanoparticles. *Nanoscale Horiz.* **2021**, *6*, 209–230. [[CrossRef](#)] [[PubMed](#)]
44. Wijngaarden, J.T.V.; Scheidelaar, S.; Vlugt, T.J.H.; Reid, M.F.; Meijerink, A. Energy transfer mechanism for downconversion in the (Pr<sup>3+</sup>, Yb<sup>3+</sup>) couple. *Phys. Rev. B* **2010**, *81*, 155112. [[CrossRef](#)]
45. Kadam, A.R.; Mishra, G.C.; Deshmukh, A.D.; Dhoble, S.J. Enhancement of blue emission in Ce<sup>3+</sup>, Eu<sup>2+</sup> activated BaSiF<sub>6</sub> downconversion phosphor by energy transfer mechanism: A photochromic phosphor. *J. Lumin.* **2021**, *229*, 117676. [[CrossRef](#)]
46. Gupta, S.K.; Garcia, M.A.P.; Zuniga, J.P.; Abdou, M.; Mao, Y.B. Visible and ultraviolet upconversion and near infrared downconversion luminescence from lanthanide doped La<sub>2</sub>Zr<sub>2</sub>O<sub>7</sub> nanoparticles. *J. Lumin.* **2019**, *214*, 116591. [[CrossRef](#)]
47. Zhang, Z.; Ma, N.N.; Kang, X.; Li, X.P.; Yao, S.Q.; Han, W.J.; Chang, H. Switchable up and down-conversion luminescent properties of Nd-nanopaper for visible and near-infrared anti-counterfeiting. *Carbohydr. Polym.* **2020**, *252*, 117134. [[CrossRef](#)]
48. Qi, H.N.; Yang, L.; Tang, X.H.; Xie, Y.R.; Ma, Q.L.; Yu, W.S.; Dong, X.T.; Li, D.; Liu, G.X.; Wang, J.X. Electrospun light stimulus response-enhanced anisotropic conductive Janus membrane with up/down-conversion luminescence. *Mater. Chem. Front.* **2022**, *6*, 2219–2232. [[CrossRef](#)]
49. Min, Q.H.; Zhao, L.; Qi, Y.S.; Lei, J.; Chen, W.B.; Xu, X.H.; Zhou, D.C.; Qiu, J.B.; Yu, X. Modified surface states of NaGdF<sub>4</sub>:Yb<sup>3+</sup>/Tm<sup>3+</sup> up-conversion nanoparticles via a post-chemical annealing process. *Nanoscale* **2018**, *10*, 19031–19038. [[CrossRef](#)]

50. Liu, Q.X.; Chen, Z.Y.; Hong, F.; Liu, G.X.; Yu, W.S.; Song, C.; Wang, J.X.; Dong, X.T. Multifunctional  $\beta$ -NaGdF<sub>4</sub>: Ln<sup>3+</sup> (Ln = Yb/Er/Eu) phosphors synthesized by L-arginine assisted hydrothermal method and their multicolor tunable luminescence. *Mater. Res. Bull.* **2019**, *110*, 141–148. [[CrossRef](#)]
51. Qiang, Q.P.; Du, S.S.; Ma, X.L.; Chen, W.B.; Zhang, G.Y.; Wang, Y.H. A temperature sensor based on the enhanced upconversion luminescence of Li<sup>+</sup> doped NaLuF<sub>4</sub>:Yb<sup>3+</sup>, Tm<sup>3+</sup>/Er<sup>3+</sup> nano/microcrystals. *Dalton Trans.* **2018**, *47*, 8656–8662. [[CrossRef](#)]
52. Jia, Q.N.; Zhang, Q.W.; Sun, H.Q.; Li, Y.; Hao, X.H. Multicolor and multimode luminescent modulation via energy transfer engineering in Tb<sup>3+</sup>/Eu<sup>3+</sup> co-doped (K<sub>0.5</sub>Na<sub>0.5</sub>)NbO<sub>3</sub> transparent photochromic materials. *J. Alloys Compd.* **2021**, *873*, 159852. [[CrossRef](#)]
53. Zou, Q.; Marcelot, C.; Ratel-Ramond, N.; Yi, X.; Roblin, P.; Frenzel, F.; Resch-Genger, U.; Eftekhari, A.; Bouchet, A.; Coudret, C.; et al. Heterogeneous oxysulfide@fluoride core/shell nanocrystals for upconversion-based nanothermometry. *ACS Nano* **2022**, *16*, 12107–12117. [[CrossRef](#)]
54. Zhou, C.; Tu, D.; Han, S.; Zhang, P.; Wang, L.P.; Yu, S.H.; Xu, J.; Li, R.; Chen, X.Y. Enhancing multi-photon upconversion emissions through confined energy migration in lanthanide-doped Cs<sub>2</sub>NaYF<sub>6</sub> nanoplatelets. *Nanoscale* **2021**, *13*, 9766–9772. [[CrossRef](#)]
55. Zhang, C.X.; Chen, J.Y.; Kong, L.M.; Wang, L.; Chen, W.; Mao, R.D.; Turyanska, L.; Jia, G.H.; Yang, X.Y. Core/shell metal halide perovskite nanocrystals for optoelectronic applications. *Adv. Funct. Mater.* **2021**, *31*, 2100438. [[CrossRef](#)]
56. Ding, M.Y.; Dong, B.; Lu, Y.; Yang, X.F.; Yuan, Y.J.; Bai, W.F.; Wu, S.T.; Ji, Z.G.; Lu, C.H.; Zhang, K.; et al. Energy manipulation in lanthanide-doped core-shell nanoparticles for tunable dual-mode luminescence toward advanced anti-counterfeiting. *Adv. Mater.* **2020**, *32*, 2002121. [[CrossRef](#)]
57. Zhao, X.Y.; Wang, M.F.; Cai, Z.W.; Xia, D.Y.; Zhao, L.; Song, Q.W.; Qin, Y.R.; Wei, W. Optimizing the performance of dye-sensitized upconversion nanoparticles. *Dye. Pigment.* **2021**, *192*, 109428. [[CrossRef](#)]
58. Kaur, M.; Mandl, G.A.; Maurizio, S.L.; Essitore, G.; Capobianco, J.A. On the photostability and luminescence of dye-sensitized upconverting nanoparticles using modified IR820 dyes. *Nanoscale Adv.* **2022**, *4*, 608–618. [[CrossRef](#)] [[PubMed](#)]
59. Liang, T.; Wang, Q.R.; Li, Z.; Wang, P.P.; Wu, J.J.; Zuo, M.M.; Liu, Z.H. Removing the obstacle of dye-sensitized upconversion luminescence in aqueous phase to achieve high-contrast deep imaging in vivo. *Adv. Funct. Mater.* **2020**, *30*, 1910765. [[CrossRef](#)]
60. Zou, J.F.; Zhu, Q.; Li, X.D.; Sun, X.D.; Li, J.G. Controlled hydrothermal processing of multiform (Y<sub>0.95</sub>Eu<sub>0.05</sub>)PO<sub>4</sub> crystals and comparison of photoluminescence. *J. Alloys Compd.* **2021**, *870*, 159380. [[CrossRef](#)]
61. Wu, S.L.; Meng, Z.P.; Sun, X.Q.; Zhang, S.F. Morphology control of the NaGdF<sub>4</sub>: Yb, Tm@NaGdF<sub>4</sub> core-shell nanostructure by tailoring the ratio of core to shell. *CrystEngComm* **2017**, *19*, 5022–5027. [[CrossRef](#)]
62. Hediger Borges, F.; Caixeta, F.J.; Pereira, R.R.; Oliveira, S.R.; Gonçalves, R.R. Yttrium tantalate containing high concentrations of Eu<sup>3+</sup> as dopant: Synthesis and structural and luminescence features. *J. Lumin.* **2018**, *199*, 143–153. [[CrossRef](#)]
63. Meenambal, R.; Kannan, S. Cosubstitution of lanthanides (Gd<sup>3+</sup>/Dy<sup>3+</sup>/Yb<sup>3+</sup>) in  $\beta$ -Ca<sub>3</sub>(PO<sub>4</sub>)<sub>2</sub> for upconversion luminescence, CT/MRI multimodal imaging. *ACS Biomater. Sci. Eng.* **2018**, *4*, 47–56. [[CrossRef](#)]
64. An, Z.C.; Zou, H.F.; Xu, C.Y.; Zhang, X.T.; Dong, R.J.; Sheng, Y.; Zheng, K.Y.; Zhou, X.Q.; Song, Y.H. Ca<sub>20</sub>Al<sub>26</sub>Mg<sub>3</sub>Si<sub>3</sub>O<sub>68</sub>:Ce<sup>3+</sup>, Tb<sup>3+</sup> phosphors: Preferential site occupation, color-tunable luminescence and device application. *ACS Sustain. Chem. Eng.* **2019**, *7*, 3154–3163. [[CrossRef](#)]
65. Yang, B.; Liu, W.W.; Choi, D.; Li, Z.C.; Cheng, H.; Tian, J.G.; Chen, C.Q. High-performance transmission structural colors generated by hybrid metal-dielectric metasurfaces. *Opt. Mater.* **2021**, *9*, 2100895. [[CrossRef](#)]
66. Ma, D.N.; Li, Z.C.; Liu, W.W.; Geng, G.Z.; Cheng, H.; Li, J.J.; Tian, J.G.; Chen, S.Q. Deep-learning enabled multicolor meta-holography. *Opt. Mater.* **2022**, *10*, 2102628. [[CrossRef](#)]
67. AlQattan, B.; Doocey, J.; Ali, M.; Ahmed, I.; Salih, A.; Alam, F.; Bajgrowicz-Cieslak, M.; Yetisen, K.A.; Elsherif, M.; Butt, H. Direct printing of nanostructured holograms on consumable substrates. *ACS Nano* **2021**, *15*, 2340–2349. [[CrossRef](#)] [[PubMed](#)]
68. Chen, F.Q.; Wang, Y.X.; Wang, S.S.; Zhai, B.X.; Lu, X.L.; Sun, B.; Ding, T. Plasmon-assisted nanopoling of poly(vinyl difluoride) films. *Opt. Mater.* **2021**, *9*, 2100084. [[CrossRef](#)]
69. Li, X.M.; Guo, Z.Z.; Zhao, T.C.; Lu, Y.; Zhou, L.; Zhao, D.Y.; Zhang, F. Filtration shell mediated power density independent orthogonal excitations–emissions upconversion luminescence. *Angew. Chem. Int. Ed.* **2016**, *55*, 2464–2469. [[CrossRef](#)] [[PubMed](#)]
70. Dong, H.; Sun, L.D.; Feng, W.; Gu, Y.Y.; Li, F.Y.; Yan, C.H. Versatile spectral and lifetime multiplexing nanoplatfom with excitation orthogonalized upconversion luminescence. *ACS Nano* **2017**, *11*, 3289–3297. [[CrossRef](#)]
71. Li, Z.Q.; Liu, X.; Wang, G.N.; Li, B.; Chen, H.Z.; Li, H.R.; Zhao, Y.L. Photoresponsive supramolecular coordination polyelectrolyte as smart anticounterfeiting inks. *Nat. Commun.* **2021**, *12*, 163. [[CrossRef](#)] [[PubMed](#)]
72. Du, K.M.; Zhang, M.L.; Li, Y.; Li, H.W.; Liu, K.; Li, C.Y.; Feng, J.; Zhang, H.J. Embellishment of upconversion nanoparticles with ultrasmall perovskite quantum dots for full-color tunable, dual-modal luminescence anticounterfeiting. *Opt. Mater.* **2021**, *9*, 2100814. [[CrossRef](#)]
73. Xie, Y.; Sun, G.T.; Song, Y.P.; Hu, P.F.; Artur, B.; Sun, L.N. Lanthanide-doped heterostructured nanocomposites toward advanced optical anti-counterfeiting and information storage. *Light-Sci. Appl.* **2022**, *11*, 150. [[CrossRef](#)] [[PubMed](#)]
74. Huang, P.R.; Wen, Z.H.; Yu, Y.; Xiao, J.Y.; Wei, Z.H.; Lyu, T.S. High charge carrier storage capacity and wide range X-rays to infrared photon sensing in LiLuGeO<sub>4</sub>:Bi<sup>3+</sup>, Ln<sup>3+</sup> (Ln = Pr, Tb, or Dy) for anti-counterfeiting and information storage applications. *Mater. Chem. Front.* **2022**, *7*, 168–182. [[CrossRef](#)]

75. Xu, L.N.; Zheng, H.Y.; Pang, T.; Mao, J.W. Multicolor luminescence of hexagonal  $\text{NaYF}_4:\text{Yb}^{3+}/\text{Ho}^{3+}/\text{Ce}^{3+}$  microcrystals with tunable morphology under 940 nm excitation for temperature-responsive anti-counterfeiting. *J. Rare Earths* **2021**, *40*, 406–414. [[CrossRef](#)]
76. Chen, Z.Y.; Yang, J.X.; Xu, R.; Zhao, Z.J.; Sang, X.; Liu, L.S.; Feng, M.; Song, F.; He, Y.H.; Huang, W. Programmable broadband responsive lanthanide-doped nanoarchitecture for information encryption. *Adv. Opt. Mater.* **2021**, *10*, 2101843. [[CrossRef](#)]
77. Wang, J.; Ma, J.; Zhang, J.C.; Fan, Y.; Wang, W.X.; Sang, J.K.; Ma, Z.D.; Li, H.H. Advanced dynamic photoluminescent material for dynamic anticounterfeiting and encryption. *ACS Appl. Mater. Interfaces* **2019**, *11*, 35871–35878. [[CrossRef](#)] [[PubMed](#)]
78. Tian, S.L.; Feng, P.; Ding, S.S.; Wang, Y.J.; Wang, Y.H. A color-tunable persistent luminescence material  $\text{LiTaO}_3:\text{Pr}^{3+}$  for dynamic anti-counterfeiting. *J. Alloys Compd.* **2022**, *899*, 163325. [[CrossRef](#)]
79. Zhang, J.C.; Pan, C.; Zhu, Y.F.; Zhao, L.Z.; He, H.W.; Liu, X.F.; Qiu, J.R. Achieving thermo-mechano-opto-responsive bitemporal colorful luminescence via multiplexing of dual lanthanides in piezoelectric particles and its multidimensional anticounterfeiting. *Adv. Mater.* **2018**, *30*, 1804644. [[CrossRef](#)]

**Disclaimer/Publisher's Note:** The statements, opinions and data contained in all publications are solely those of the individual author(s) and contributor(s) and not of MDPI and/or the editor(s). MDPI and/or the editor(s) disclaim responsibility for any injury to people or property resulting from any ideas, methods, instructions or products referred to in the content.